

Unsupervised Collaborative Metric Learning with Mixed-Scale Groups for General Object Retrieval

Shichao Kan, Yuhai Deng, Yixiong Liang, Lihui Cen, Zhe Qu, Yigang Cen, and Zhihai He

Abstract—The task of searching for visual objects in a large image dataset is difficult because it requires efficient matching and accurate localization of objects that can vary in size. Although the segment anything model (SAM) offers a potential solution for extracting object spatial context, learning embeddings for local objects remains a challenging problem. This paper presents a novel unsupervised deep metric learning approach, termed unsupervised collaborative metric learning with mixed-scale groups (MS-UGCML), devised to learn embeddings for objects of varying scales. Following this, a benchmark of challenges is assembled by utilizing COCO 2017 and VOC 2007 datasets to facilitate the training and evaluation of general object retrieval models. Finally, we conduct comprehensive ablation studies and discuss the complexities faced within the domain of general object retrieval. Our object retrieval evaluations span a range of datasets, including BelgaLogos, Visual Genome, LVIS, in addition to a challenging evaluation set that we have individually assembled for open-vocabulary evaluation. These comprehensive evaluations effectively highlight the robustness of our unsupervised MS-UGCML approach, with an object level and image level mAPs improvement of up to 6.69% and 10.03%, respectively. The code is publicly available at <https://github.com/dengyuhai/MS-UGCML>.

Index Terms—Open vocabulary object retrieval, unsupervised metric learning, image retrieval, deep metric learning.

I. INTRODUCTION

OBJECT retrieval [1], [2] is crucial for locating specific targets in a large-scale visual corpus. It involves retrieving similar images containing a given object and determining the object's spatial location. This task is replete with challenges, primarily because target objects tend to exist

This work was supported in part by the National Natural Science Foundation of China under Grant 62202499, in part by the State Key Program of National Natural Science Foundation of China under Grant 62233018, in part by the Beijing Natural Science Foundation under grant L231012, in part by the Hunan Provincial Natural Science Foundation of China under Grant 2022JJ40632. We are grateful to the High Performance Computing Center of Central South University for partial support of this work. (Corresponding author: Yuhai Deng)

Shichao Kan, Yixiong Liang, and Zhe Qu are with the School of Computer Science and Engineering, Central South University, 410083, Changsha, Hunan, China (e-mail: kanshichao@csu.edu.cn, yxliang@csu.edu.cn, zhe_qu@csu.edu.cn).

Yuhai Deng and Lihui Cen are with the School of Automation, Central South University, 410083 Changsha, Hunan, China (e-mail: yuhai_deng@csu.edu.cn; lhcen@csu.edu.cn).

Yigang Cen is with the Institute of Information Science, School of Computer and Information Technology, Beijing Jiaotong University, Beijing 100044, China, and also with the Beijing Key Laboratory of Advanced Information Science and Network Technology, Beijing 100044, China (e-mail: ygcn@bjtu.edu.cn).

Zhihai He is with the Department of Electrical and Electronic Engineering, Southern University of Science and Technology, Shenzhen, China, and also with the Pengcheng Lab, Shenzhen 518066, China (e-mail: hezh@sustech.edu.cn).

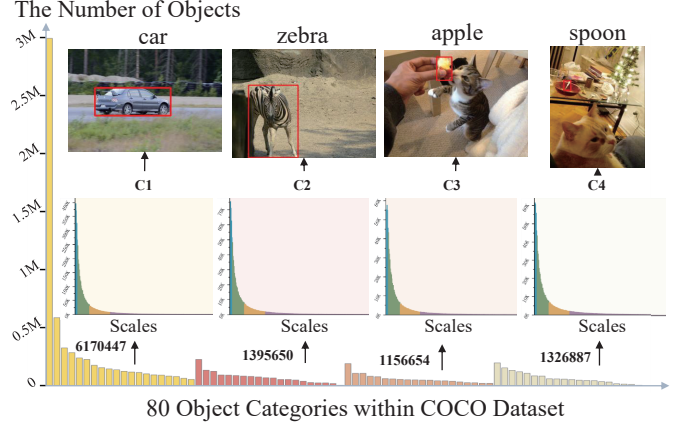


Fig. 1. Scale distributions in an open-world scenario: analyzing 4 sets of 80 object classes with long-tailed distributions. The x-axis represents scales and the y-axis represents the number of examples in the four sub-images.

within cluttered backgrounds, occupy relatively small and unpredictable portions of an image, and can exhibit significant deviations from the query due to variations in factors such as scale, viewpoint, color, and partial occlusions. Most of the existing literature on object retrieval algorithms has primarily been developed for specific object retrieval tasks, such as person re-identification [3]–[5], vehicle re-identification [6], [7], clothing retrieval [8], and logo retrieval [1]. In these tasks, the distribution of objects follows an independent and identically distributed (*i.i.d.*) pattern, limiting the algorithms' ability to generalize to non-*i.i.d.* tasks. For instance, an algorithm developed based on pedestrian datasets may perform well on person retrieval tasks but may not generalize effectively to vehicle retrieval tasks. In this paper, our objective is to develop an algorithm for general object retrieval, encompassing both seen and unseen objects.

In the context of general object retrieval, addressing the long-tailed distribution of objects is one of the primary challenges. This distribution pattern is a common occurrence in open-world scenarios, as illustrated in Fig. 1. The majority of objects are concentrated within the head classes, making it more challenging to recognize or retrieve objects from the tail classes [9]. Furthermore, it's important to note that the scale distribution also exhibits a long-tailed pattern, as demonstrated in the sub-distributions of Fig. 1. This presents an additional challenge as it becomes difficult to learn effective embeddings for small scale objects under unsupervised conditions. Prior research primarily focused on tackling the long-tailed issue related to the number of objects. However, the long-tailed problem associated with the scale of objects was not addressed

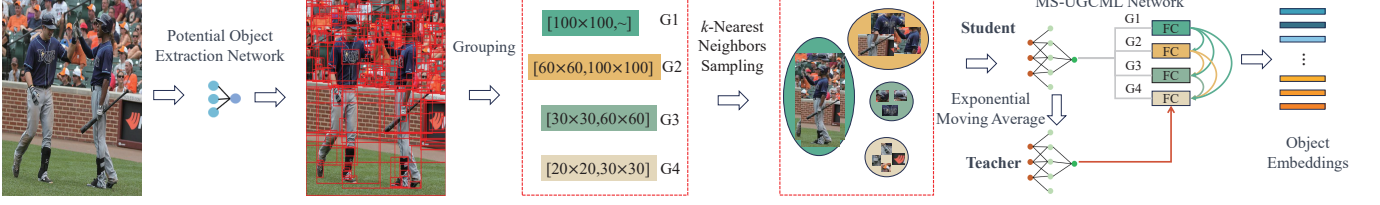


Fig. 2. The pipeline for general object embedding learning using unsupervised collaborative metric learning with mixed-scale groups (MS-UGCML) method.

in previous work.

As depicted in Fig. 1, the majority of objects are characterized by large sizes. However, in dynamic and open environments, most previously unseen objects belong to the tailed classes and possess small scales. This introduces challenges in the extraction and representation of such objects. While the segment anything model (SAM) [10] offers a potential solution for capturing object spatial context, and unsupervised representation learning algorithms like DINO [11], MoCo [12], iBOT [13], and STML [14] have demonstrated impressive performance in general image representation, employing these methods to obtain representations of open-vocabulary and small-scale objects may result in a degradation of performance.

To tackle the long-tailed problem associated with the scale of objects, this paper introduces an unsupervised collaborative metric learning with mixed-scale groups (MS-UGCML) method, designed to effectively learn object embeddings, as illustrated in Fig. 2. The approach includes a potential object extraction network for object extraction and an MS-UGCML network for object embedding learning. The potential object extraction network could be a general object extraction network, such as MViT [15] or SAM [10]. Because SAM has been trained on a dataset of 10 million images, it exhibits the capability to perform hierarchical object segmentation, allowing for the extraction of various objects. Consequently, in this work, we harness SAM's potential to extract objects from images, with the goal of achieving open-vocabulary object retrieval. The MS-UGCML network can be configured using popular CNN-based or Transformer-based networks. In our experiments, we explored various backbone networks.

Furthermore, existing datasets used for deep feature embedding, such as ImageNet [16], SOP [17], CUB [18], and Cars [19], primarily consist of images with uniform sizes. These samples may diverge considerably from those encountered in dynamic real-world scenarios. Conversely, datasets employed for image retrieval tasks, like Oxford5k [20] and Paris6k [21], enable the evaluation of retrieval performance for specific object categories. They fall short when it comes to training a model to represent a diverse range of objects. To better mimic real-world applications, we curate a new dataset by amalgamating data from COCO 2017 [22] and VOC 2007 [23] datasets. This dataset serves as a valuable resource for training and evaluating open-vocabulary object retrieval models. Importantly, there are no strict category constraints imposed on either the training or test samples. Consequently, the model is trained on samples with uncertain categories and tested on samples with uncertain categories as well. To assess the generalization capability of the model, we

conducted additional testing on a range of datasets, including BelgaLogos [24], Visual Genome [25], and LVIS [26] datasets. The contributions of this work are summarized as follows:

- We introduce an unsupervised collaborative metric learning with mixed-scale groups method for general object retrieval. The core concept involves the grouping of various objects based on their sizes, and then calculating Euclidean distances to generate losses for each group. Additionally, we employ distance distillation between different groups to further refine the model.
- We construct a benchmark of challenges by leveraging data from COCO 2017 [22] and VOC 2007 [23] datasets, facilitating the training and evaluation of general object retrieval models. Furthermore, we assemble a rigorous test set specifically designed for evaluating open-set object retrieval performance.
- In addition to our internally curated evaluation set, our object retrieval assessments encompass a variety of datasets, including BelgaLogos [24], Visual Genome [25], and LVIS [26]. The results demonstrate that our proposed MS-UGCML method substantially enhances feature embedding performance when compared to the baseline methods, resulting in an object- and image-level mAP improvement of up to 6.69% and 10.03%, respectively.

II. RELATED WORK

The task of visual object retrieval, which involves identifying and accurately locating target objects within image collections, remains a formidable challenge with a well-established research history. In the following subsections, we provide an overview of prior work related to this topic, encompassing object matching and object localization.

A. Object Matching

Early approaches frequently employed for object matching include the bag-of-visual-words (BoVW) [27] and vector of locally aggregated descriptors (VLAD) [28]. These methods follow a two-stage pipeline where individual descriptors in the feature space are matched initially and then aggregated for object matching. Matching individual descriptors in this manner can potentially introduce quantization errors, thereby degrading the object-matching performance. To mitigate quantization errors, spatial context, which involves grouping co-occurring visual words within a constrained spatial distance into a visual phrase [1], [29] or feature group [30], is used as the fundamental unit for object matching. The primary

limitations of these methods are their high memory and time requirements since they involve the extraction and matching of local descriptors. Recent studies have generated visual representations from the activations of convolutional layers [31] and transformer blocks [7]. These studies extensively utilized deep metric learning methods.

Deep metric learning aims to learn discriminative features from images by minimizing the distance between samples of the same class and maximizing the distance between samples of different classes. In early deep metric learning methods, contrastive loss [32] was effectively employed to optimize the pairwise distances between samples. To explore more intricate relationships between samples, various metric loss functions, including triplet loss [33] and lifted structured loss [34], have been developed. These methods rely on supervised learning using image labels. However, in real-world object retrieval scenarios, objects are often unknown and lack labels. To learn representations of unlabeled objects, several techniques have been proposed. He *et al.* [35] introduced the momentum contrast (MoCo) method for unsupervised visual representation learning. Chen *et al.* [36] presented the simCLR framework, which is based on contrastive learning, for effective unsupervised visual representation learning.

In an effort to generate more robust pseudo-labels for unsupervised deep metric learning, Nguyen *et al.* [37] introduced a deep clustering loss to learn centroids. More recently, Kan *et al.* [38] proposed a relative order analysis (ROA) and optimization method for enhancing the relative ranking of examples in unsupervised deep metric learning. Li *et al.* [39] developed spatial assembly networks (SAN) to facilitate both supervised and unsupervised deep metric learning. Kim *et al.* [14] introduced an effective teacher-student learning pipeline for embedding learning of unlabeled images.

The methods mentioned above have primarily been investigated using evenly distributed class examples with images of the same size. Their performance may deteriorate when applied to real-world datasets with long-tailed distributions and varying image sizes. Our work aims to develop a general object embedding method that is more representative of the real world, setting it apart from the aforementioned works.

B. Object Localization

In previous object localization methods, images are initially retrieved, followed by the determination of the object's location using bounding boxes on matched regions in a post-processing step, typically through geometric verification techniques like RANSAC [20] or neighboring feature consistency [40]. Since geometric verification methods can be computationally expensive, they are usually applied to only the top-ranked images in the initial retrieval list. As an alternative, efficient subimage retrieval (ESR) [41] and efficient subwindow search (ESS) [42] were introduced to identify the subimage with the highest similarity to the query. Additionally, spatial random partitioning was proposed in [1] to discover and locate common visual objects.

Recently, object detection methods such as YOLO [43], Faster R-CNN [44], MViT [15], and SAM [10] were used to

detect and locate objects in the image. Among these methods, SAM [10] demonstrates robustness in extracting objects in open-world scenarios. In our work, we also leverage SAM for both the extraction and localization of objects before and after the object retrieval process.

III. CHALLENGES AND MOTIVATION IN GENERAL OBJECT RETRIEVAL

Unlike object detection, which aims to recognize and locate objects within an image, object retrieval is focused on ranking images and locating objects within the retrieved images. Typically, object detection algorithms are employed as the initial step in object retrieval to extract objects. In real-world scenarios, object retrieval introduces a new challenge: the query object can be any object, making the extraction and retrieval of arbitrary objects a challenging task. To address this challenge, previous state-of-the-art methods have introduced approaches like MViT [15] and SAM [10] for extracting both known and unknown objects. However, the representation of objects for retrieval remains an area that has not been thoroughly explored. To investigate this matter, we conducted experiments using the state-of-the-art unsupervised STML [14] method based on MViT and SAM. These experiments were conducted using our carefully curated training and validation sets, which consist of a total of 80 classes from COCO 2017 [22] and VOC 2007 [23].

To simulate an open-world scenario, we followed the dataset partitioning in [45] and divided the dataset into 4 tasks, denoted as Task1 to Task4, with each task progressively adding 20 new classes. The model is trained on each task and subsequently evaluated under three different scenarios: close-set (known), open-set (unknown), and open-vocabulary (all). In this context, “known” signifies that the test classes match the training classes, “unknown” indicates that the test classes are distinct from the training classes, and “all” denotes that the model is tested on all 80 classes. The results on the validation set are presented in Fig. 3 (a)-(c). It is apparent that, as we progress from Task1 to Task4, the object-level retrieval mAP scores exhibit a consistent decrease for both the MViT and SAM extraction methods across all three scenarios. The observed decline in object-level retrieval mAP scores within the close-set and open-set scenarios can be attributed to the challenges posed by the introduction of new class samples. Additionally, for known objects (Fig. 3 (a)), the object-level mAP scores based on SAM are lower compared to those based on MViT. This can be attributed to the significantly higher number of objects extracted by SAM (averaging 89 per image) in comparison to MViT (averaging 14 per image).

However, from Fig. 3 (c), we have observed that the inclusion of more class samples also results in a decrease in object-level mAP scores within the open-vocabulary scenario. Upon conducting a thorough analysis of the underlying causes of this phenomenon, we have discerned two principal contributing factors. The first factor pertains to the inherent properties of the newly added classes, specifically their relatively smaller object sizes. This characteristic can exacerbate the challenges of unsupervised training by introducing a heightened susceptibility to labeling errors. As demonstrated in Fig. 3 (d), the

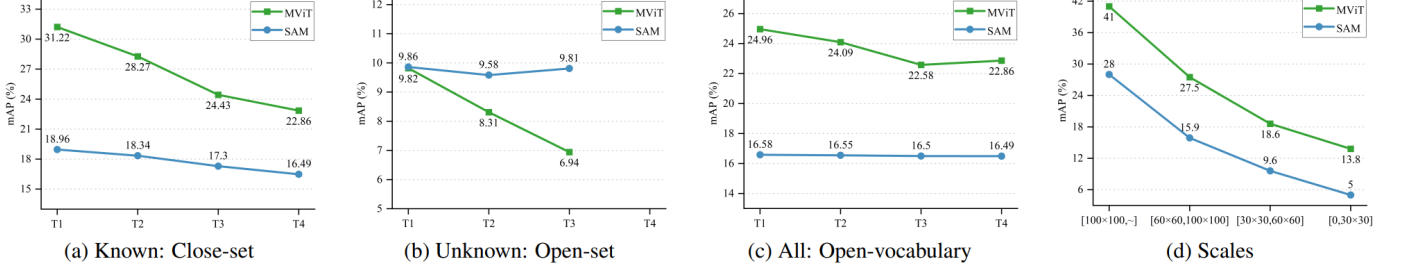


Fig. 3. Retrieval scores (%) at the object level with different object extraction methods on the validation set for object retrieval, considering known, unknown, all, and objects of different scales.

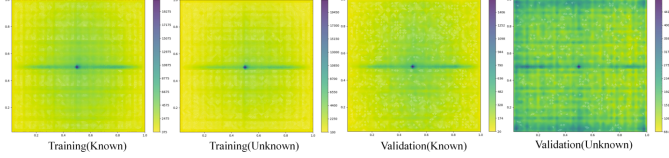


Fig. 4. Spatial distributions of known and unknown objects within both the training and validation sets for Task1.

retrieval mAP score decreases with the smaller scale of the query object. The second factor pertains to the distinct spatial distribution characteristics exhibited by the newly incorporated classes in comparison to the known classes. As illustrated in Fig. 4, the spatial distributions of the unknown objects differ between the training and validation sets. These variations in spatial attributes further compound the challenges encountered within this open-vocabulary scenario. In response to these challenges, we introduce a novel unsupervised collaborative metric learning with mixed-scale groups method designed to learn models for general object representation. Furthermore, it is observed that the unknown object retrieval mAP scores (Fig. 3 (b)) consistently outperform when utilizing the SAM for object extraction as compared to the MViT approach. Consequently, SAM is adopted as the preferred object extraction method in our experiments.

IV. METHODS

This paper focuses on achieving general object retrieval. In the following subsections, we introduce our proposed method, unsupervised collaborative metric learning with mixed-scale groups (MS-UGCML), to attain this objective.

A. Method Overview

Fig. 5 offers an overview of the MS-UGCML method proposed for object retrieval. Our primary objective, as shown in the object retrieval pipeline, is to train a universal object embedding network capable of representing any object. This network enables the extraction of embeddings for both query and gallery objects. Subsequently, we compute the Euclidean distances between the query embedding and the gallery embeddings. These distances are used for ranking, resulting in the retrieval of the top-k objects, which are then located within their respective images. To train the object

embedding network, we employ two embedding networks, a teacher network ϕ^t and a student network ϕ^s , each sharing the same backbone and having identically initialized parameters. The process begins with the extraction of unlabeled objects from the training images using SAM [10]. These objects are then sampled at various scales to form batches, which are input into both the teacher network ϕ^t and the student network ϕ^s .

The teacher network ϕ^t is responsible for estimating semantic similarities between pairs of samples. These similarity estimates are subsequently used as synthetic supervision for training the student network. The student network ϕ^s consists of multiple parallel heads (e.g., 2, 3, or 4), each containing two parallel embedding layers: h_m^s and l_m^s , where m is a group index. Both the backbone and the embedding layer h^t of the teacher network are maintained as exponential moving averages of their corresponding parts in the student network. h^t and h_m^s have higher dimensions (e.g., 1024) to encode richer information and generate more reliable semantic similarities. h_m^s is an auxiliary layer and dedicated to continually updating the teacher embedding layer h^t . The embedding layer l_m^s in our final model has a lower dimension (e.g., 512) to learn a compact embedding space.

Following the heads of the student network, we proceed to compute Euclidean distances for each group of output embeddings. Subsequently, we compute the self-distillation loss $\mathcal{L}_m^{\text{self}}$ by comparing the distances calculated from the output embeddings of h_m^s and l_m^s . Additionally, we determine the relaxed contrastive loss $\mathcal{L}_m^{\text{con}}$ based on the Euclidean distances computed from the output embeddings of h_m^s and l_m^s , respectively. Lastly, we compute the collaborative knowledge distillation loss \mathcal{L}_{CKD} between different groups. Our MS-GCML loss function $\mathcal{L}_{\text{MS-UGCML}}$ is constructed by aggregating all of these loss functions. This combined loss function guides the parameter updates of the student network in an end-to-end manner. The details of each part are described in the following sections.

B. Unsupervised Collaborative Metric Learning with Mixed-Scale Groups

Fig. 6 portrays the intricate pipeline of our MS-UGCML. As elaborated upon in Sec. III, the effectiveness of embedding learning is closely associated with the accuracy of labeling, which, in turn, is linked to the scale of the image. Generally, images with larger scales tend to yield higher labeling

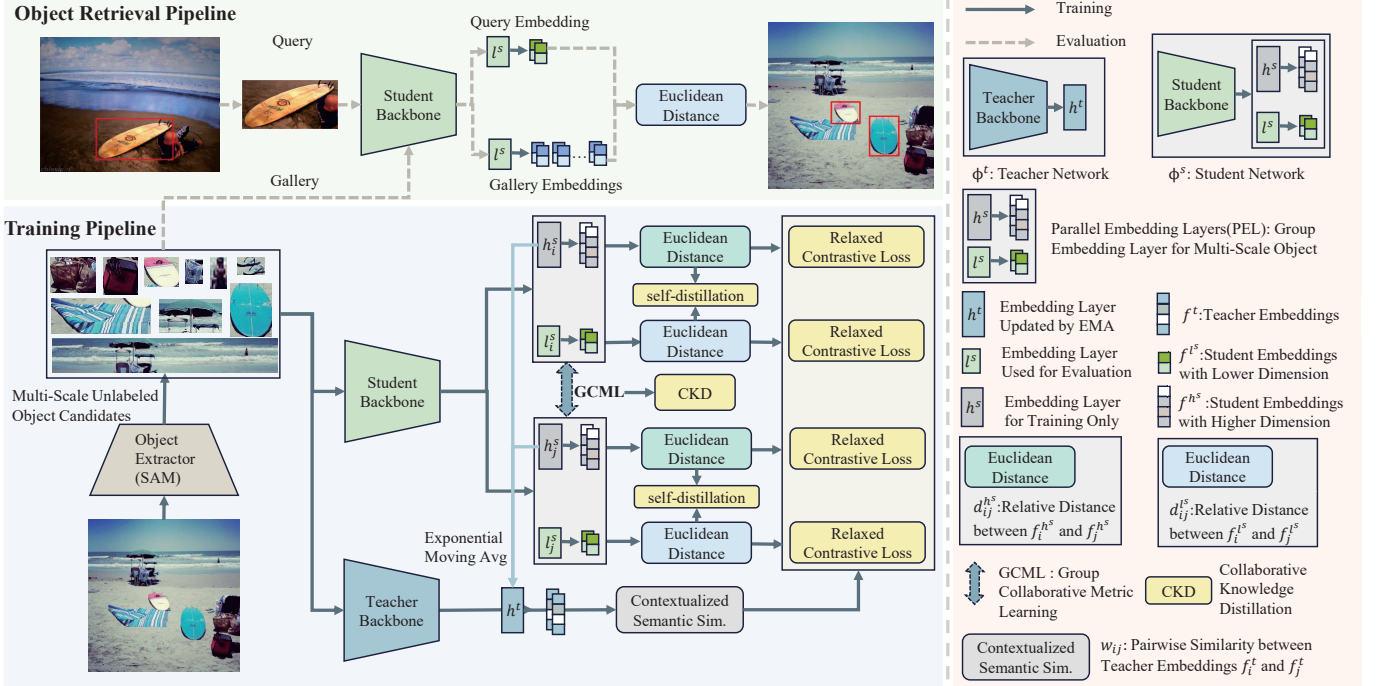


Fig. 5. An overview of our object retrieval and object embedding training pipeline. A teacher-student training strategy is employed during the training process. Firstly, we estimate contextualized semantic similarity between data pairs in the embedding space of the teacher network. Then, unsupervised collaborative metric learning with mixed-scale groups is utilized to update the parameters of the student network. Ultimately, the trained student network is employed in the object retrieval process.

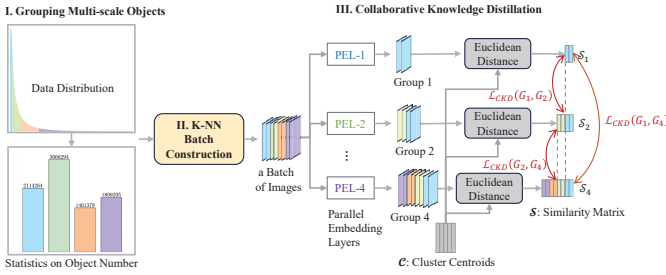


Fig. 6. The pipeline of unsupervised collaborative metric learning with mixed-scale groups (MS-UGCML).

accuracy, while those with smaller scales may result in lower labeling accuracy.

Building upon the preceding analysis, we propose categorizing images according to their sizes. As depicted in the initial step of Fig. 6, the data distribution exhibits a long-tailed nature. The horizontal axis represents the image sizes, arranged from small to large, while the vertical axis denotes the number of objects. To uniformly sample data across different scales, we segment this data into multiple groups with uniform distributions (e.g., 4), spanning from small to large based on image area.

Then, we explore the use of k -nearest neighbors (K-NN) to sample data from each group, forming a batch of images, as illustrated in the second step of Fig. 6. Subsequently, we compute the collaborative knowledge distillation loss based on the grouped embeddings. Specifically, for the m -th group, we denote the student output embedding vectors generated by l_m^s as $\mathcal{F}^{l_m^s}$. To initiate the process, we employ the k-means

clustering algorithm to cluster all the training embeddings, resulting in a set of clustering centroids, denoted as \mathcal{C} . We then compute the normalized similarity matrix S_m between embeddings in group m and cluster centroids in \mathcal{C} . For collaborative knowledge distillation (CKD) between group a and group b , we utilize the Kullback-Leibler divergence to calculate their CKD loss, which is defined as follows

$$\mathcal{L}_{CKD}(G_a, G_b) = \frac{1}{|G_{a \cap b}|} \sum_{o_i \in G_{a \cap b}} \mathcal{L}_{KL}(S_a^i, S_b^i).$$

In the formula, G_a and G_b represent the object image sets in group a and b , while $G_{a \cap b}$ denotes the set of identical object images found in both group a and b . The term $|G_{a \cap b}|$ corresponds to the number of images in $G_{a \cap b}$. S_a^i represents the indexed similarity vector between the embeddings of object o_i and \mathcal{C} within the matrix S_a . The function of Kullback-Leibler divergence $\mathcal{L}_{KL}(S_a^i, S_b^i)$ is defined as follows

$$\mathcal{L}_{KL}(S_a^i, S_b^i) = - \sum_{l=1}^L S_a^i(l) \log S_b^i(l), \quad (1)$$

where $L = |\mathcal{C}|$, which is the total similarities between the embeddings of object o_i , and \mathcal{C} . Finally, the CKD loss in all groups is computed as follows

$$\mathcal{L}_{CKD} = \frac{1}{|\mathcal{Q}|} \sum_{(a, b) \in \mathcal{Q}} \mathcal{L}_{CKD}(G_a, G_b), \quad (2)$$

where $|\mathcal{Q}|$ is calculated as $|\mathcal{Q}| = \frac{k(k-1)}{2}$, with k representing the number of groups.

C. Overall Loss Function

To train the network, we utilize a combination of knowledge distillation and contrastive loss functions. The primary objective of the knowledge distillation loss is to extract more informative features from the more dependable embeddings. Meanwhile, the contrastive loss function serves as a metric loss, with the aim of learning a Mahalanobis distance metric. They were defined according to the following definitions. First, we define the loss functions $\mathcal{L}_m^{\text{self}}$ and $\mathcal{L}_m^{\text{con}}$ following the works of STML [14]. Let the student output embedding vectors generated by h_m^s and l_m^s in the m -th group be denoted as $\mathcal{F}^{h_m^s}$ and $\mathcal{F}^{l_m^s}$. The self-distillation loss $\mathcal{L}_m^{\text{self}}$ is computed based on Kullback-Leibler divergence, as follows:

$$\mathcal{L}_m^{\text{self}}(\mathcal{F}^{h_m^s}, \mathcal{F}^{l_m^s}) = \sum_{i=1}^n \sum_{j \neq i}^n \frac{\psi(-d_{ij}^{l_m^s})}{n} \log \frac{\psi(-d_{ij}^{l_m^s})}{\psi(-d_{ij}^{h_m^s})}, \quad (3)$$

where $d_{ij}^{l_m^s} := \|\mathbf{f}_i^{l_m^s} - \mathbf{f}_j^{l_m^s}\|_2 / (\frac{1}{n} \sum_{k=1}^n \|\mathbf{f}_i^{l_m^s} - \mathbf{f}_k^{l_m^s}\|_2)$ represents the relative distance between $\mathbf{f}_i^{l_m^s}$ and $\mathbf{f}_j^{l_m^s}$. Similarly, $d_{ij}^{h_m^s}$ represents the relative distance between $\mathbf{f}_i^{h_m^s}$ and $\mathbf{f}_j^{h_m^s}$. The function $\psi(\cdot)$ corresponds to the softmax operation, and n represents the number of samples in the m -th group. The relaxed contrastive loss $\mathcal{L}_m^{\text{con}}$ is defined as follows

$$\begin{aligned} \mathcal{L}_m^{\text{con}}(\mathcal{F}^{h_m^s}) &= \frac{1}{n} \sum_{i=1}^n \sum_{j \neq i}^n w_{ij} (d_{ij}^{h_m^s})^2 \\ &+ \frac{1}{n} \sum_{i=1}^n \sum_{j \neq i}^n (1 - w_{ij}) [\delta - d_{ij}^{h_m^s}]_+^2, \end{aligned} \quad (4)$$

where $w_{ij} = \exp(-\frac{\|\mathbf{f}_i^t - \mathbf{f}_j^t\|_2^2}{\sigma})$ represents a pairwise similarity score between teacher embeddings \mathbf{f}_i^t and \mathbf{f}_j^t , and δ is a margin. It's worth noting that the same training approach is applied to l_m^s as well. The overall loss function $\mathcal{L}_{\text{MS-UGCML}}$ is defined as follows

$$\begin{aligned} \mathcal{L}_{\text{MS-UGCML}} &= \sum_{i=1}^k \mathcal{L}_i^{\text{self}}(\mathcal{F}^{h_i^s}, \mathcal{F}^{l_i^s}) + \sum_{i=1}^k \mathcal{L}_i^{\text{con}}(\mathcal{F}^{h_i^s}) \\ &+ \sum_{i=1}^k \mathcal{L}_i^{\text{con}}(\mathcal{F}^{l_i^s}) + \mathcal{L}_{\text{CKD}}. \end{aligned}$$

V. EXPERIMENTS

A. Datasets

Our training dataset is curated from pre-existing open-access object detection datasets, i.e., COCO 2017 [22] and VOC 2007 [23]. The testing dataset consists of publicly available object retrieval and object detection datasets, which serve to evaluate the performance of general object retrieval. Their details are summarised in Table I and detailed information on these datasets is provided below.

General object retrieval dataset. The training and validation sets are constructed by extracting objects from the training sets of COCO 2017 and VOC 2007, as well as the validation set of VOC 2007. The training set comprises 121,298 images, while the validation set contains 2,000 images. The test set is composed of objects extracted from the validation set of

TABLE I
STATISTICS ON THE NUMBER OF TRAINING AND TEST SETS.

	Images	Objects
training dataset	121,298	8,035,395
COCO-VOC test query	9,904	51,757
COCO-VOC test gallery	9,904	862,861
BelgaLogos test query	55	55
BelgaLogos test gallery	10,000	939,361
LVIS test query	4726	50,537
LVIS test gallery	4726	433,671
Visual Genome test query	108,077	79,921
Visual Genome test gallery	108,077	9,803,549

COCO 2017 and the test set of VOC 2007, totaling 9,904 images. To perform object extraction, we employed SAM [10]. The resulting partitioned sets consist of more than 8 million objects for the training set, 173K for the validation set, and 862K for the test set. In the zero-shot object retrieval setup, we partition the training set into four distinct groups, with each group comprising 20 object classes. These four group datasets are employed to create four tasks, with each task progressively introducing an additional set of 20 new classes. The classes utilized for training (known classes highlighted in light yellow) and testing (unknown classes highlighted in light blue) in each task are presented in Table IX. In Task 1, the training set consists of the most popular 20 classes, while the remaining 60 classes are used for testing. For Task 2, 20 new classes are introduced along with the original Task 1 classes for training, and the remaining 40 classes are designated for testing. Task 3 involves the addition of another set of 20 new classes to Task 2, with the remaining 20 classes used for testing. Finally, Task 4 incorporates all 80 classes for both training and testing phases. The results for different tasks are shown in Fig. 3 (b).

Generalization evaluation dataset. To assess the generalization ability of the trained MS-UGCML model, we conducted evaluations on the BelgaLogos [24], Visual Genome [25], and LVIS [26] datasets. The BelgaLogos dataset consists of 10K images and 55 query logos, primarily used to evaluate the logo retrieval performance of an algorithm. The provided 55 query logo images of the BelgaLogos dataset are utilized as the query set, while the gallery set comprises 939,361 objects extracted using SAM [10]. In the case of the Visual Genome dataset, which contains 108K images and 2,516,939 labeled bounding boxes, we define a set of 79,921 objects as the query set and directly performed object retrieval using the trained model on the whole dataset. As for the LVIS dataset, it shares the same images as the COCO 2017 dataset but features 1000 class labels. We compute evaluation scores based on the labeled objects in the validation set of the LVIS dataset.

Evaluation Metrics. We use Recall@1 and mean average precision (mAP) as the evaluation metrics for object retrieval. The Recall@1 is defined as follows: $\text{Recall}@1 = \frac{1}{q} \sum_{i=1}^q r_i$, where q represents the number of queries, and r_i is equal to 1 if the top-1 returned objects contain the ground truth object, and 0 otherwise. The mAP is calculated as: $\text{mAP} = \frac{1}{q} \sum_{i=1}^q \sum_{j=1}^q \frac{j}{p_j}$, where q represents the number of queries,

TABLE II

RETRIEVAL SCORES (%) AT BOTH THE OBJECT LEVEL (O-) AND IMAGE LEVEL (I-) WITH DIFFERENT BACKBONE NETWORKS AND DIFFERENT INITIALIZATION METHODS ON THE OBJECT RETRIEVAL TEST SET.

Backbone	Methods	O-R@1	O-mAP	I-R@1	I-mAP
GoogLeNet [50]	STML [14]	65.93	14.89	69.70	65.04
	MS-UGCML	68.17	15.37	71.90	67.69
MiT-B2 [51]	STML [14]	58.62	17.48	66.86	58.60
	MS-UGCML	68.60	17.64	73.40	68.63
ViT-B/16 [48]	MoCo-V3 [12]	77.40	15.94	81.29	81.26
	MS-UGCML	77.88	16.84	82.04	82.12
	CLIP [49]	68.44	14.56	74.01	70.30
	MS-UGCML	69.07	16.07	74.49	70.97

and p_j is the ranking index of a returned object that matches the ground truth. We calculate image-level and object-level retrieval scores. The image-level score is computed using an IoU threshold of $1e^{-10}$, and the object-level score is computed using an IoU threshold of 0.3.

B. Implementation Details

In our experiments utilizing SAM [10] and MViT [15], different settings for object extraction were employed. Specifically, the ViT-H backbone network was utilized for object extraction based on SAM. For object extraction based on MViT, the text prompts 'all objects,' 'all entities,' 'all visible entities and objects,' and 'all obscure entities and objects' were employed. Our teacher-student network is trained on two RTX 3090 (24GB) GPUs with a batch size of 120. The nearest neighbors are set to 5. Each batch contains images of various sizes for MS-GCML learning. The group number of the MS-UGCML is set to 4, and the clustering number is set to 100 unless specified otherwise. The dimension of teacher embeddings f^t was set to 1024, while the dimensions of student embeddings f^{l^s} and f^{h^s} were both set to 512. The σ to calculate w_{ij} and the margin δ in Equation 4 are 3 and 1 respectively. The initial learning rate is set as 10^{-4} on the backbone of GoogLeNet, and 3×10^{-5} for MiT-B2 and ViT-B/16, both of which are scaled down by the cosine decay function [46]. During training, The Adamp [47] optimizer was employed with a weight decay set to 0.01. and the K-nearest neighbor sampling distance matrix was updated once every 1000 iterations.

C. Effectiveness Verification of the MS-UGCML Method

To assess the effectiveness of the MS-UGCML method, we conducted experiments using different backbone networks and various initialization methods. The results on the curated test set are presented in Tab. II. In this table, methods based on the GoogLeNet and MiT-B2 backbone networks are initialized with parameters trained on the ImageNet-1K [16] dataset. Our method based on the ViT-B/16 [48] backbone network are initialized using parameters trained by the MoCo-V3 [12] and CLIP [49] methods, respectively, and then fine-tuned on our curated training dataset using the proposed MS-UGCML method.

From Tab. II, it is evident that our method outperforms the state-of-the-art unsupervised STML [14] method, achieving

an improvement of 2.65% and 10.03% in image level mAP for GoogLeNet and MiT-B2 backbone networks, respectively. Additionally, it is notable that the general object retrieval score exhibits a significant disparity compared to the other metrics, underscoring the substantial potential for enhancement within the domain of object retrieval. The MS-UGCML method with the MiT-B2 backbone network obtained the highest object level mAP score.

To further verify the effect of unsupervised collaborative metric learning with mixed-scale groups (MS-UGCML), we present the results for different sizes of query objects, as shown in Tab. III and Tab. IV. Tab. III and Tab. IV show object retrieval results based on the GoogLeNet [50] backbone and the MiT [51] backbone, respectively. We can see that the MS-UGCML obtained better performance in both the object- and image-level retrieval scores for different sizes of query objects. Moreover, the larger size of objects, the higher the performance for both the STML [14] and the MS-UGCML methods.

Fig. 7 illustrates the comparison of three object retrieval examples between the MS-UGCML and STML [14] methods. The first retrieval example is based on the GoogLeNet backbone network, while the second and third retrieval examples are based on the MiT-B2 backbone network. These examples demonstrate that the MS-UGCML method is capable of returning more relevant objects associated with the query object.

D. Comparison and Analysis of General Object Retrieval

Moreover, we conduct evaluation experiments on the BelgaLogos [24], Visual Genome [25], and LVIS [26] datasets using the trained model. Results are shown in Tab. V. We have observed that our approach using GoogLeNet [50] and MiT-B2 [51] backbone networks effectively enhances retrieval performance across various datasets. The object-level mAP scores demonstrated a 6.69% improvement on the Visual Genome dataset and a 0.89% improvement on the LVIS dataset when using the MiT-B2 backbone network. The highest mAP scores and Recall@1 scores on the BelgaLogos, Visual Genome, and LVIS dataset are achieved with the parameters initialized by the MoCo-V3. However, on the Visual Genome dataset, the performance of the MS-UGCML method with MoCo-V3 slightly decreases due to the lower-dimensional feature embeddings (512 v.s. 1000).

Fig. 8 provides logo retrieval example showcasing the effectiveness of the proposed MS-UGCML method. These examples illustrate the ability to ground multiple objects within the retrieved images.

E. Ablation Study

We conducted ablation studies on our curated object retrieval dataset using the GoogLeNet [50] backbone. In the subsequent ablation experiments, we utilize objects extracted by SAM for both training and validation.

(1) **Impact of the clustering number.** We examined the impact of the clustering number on deep feature embedding performance, with the number of groups fixed at 3. The results on the validation set are presented in Tab. VI, and it's evident

TABLE III
RETRIEVAL SCORES (%) OF DIFFERENT SCALES OF QUERY OBJECTS BASED ON THE GOOGLENET BACKBONE.

Sizes	Methods	COCO-VOC				LVIS			
		O-R@1	O-mAP	I-R@1	I-mAP	O-R@1	O-mAP	I-R@1	I-mAP
[0,20 × 20]	STML [14]	14.30	1.63	20.67	15.23	21.25	2.80	22.10	24.66
	MS-UGCML	18.38	1.68	24.06	20.27	25.18	3.29	26.43	28.98
[20 × 20,30 × 30]	STML [14]	42.72	3.61	49.25	44.50	52.48	5.88	53.22	57.72
	MS-UGCML	52.20	3.75	57.11	53.64	58.77	7.01	59.58	63.89
[30 × 30,60 × 60]	STML [14]	64.51	6.91	69.22	64.83	67.22	7.40	67.77	72.46
	MS-UGCML	68.13	6.96	72.89	68.50	70.46	8.25	71.07	75.72
[60 × 60,100 × 100]	STML [14]	78.05	14.73	81.83	76.06	76.14	8.46	76.85	81.25
	MS-UGCML	79.74	15.34	83.32	78.25	78.47	9.24	79.32	83.53
[100 × 100,~]	STML [14]	85.74	26.68	87.66	83.50	81.87	11.30	82.77	86.54
	MS-UGCML	87.56	27.77	89.61	86.47	83.71	13.01	85.00	88.74

TABLE IV
RETRIEVAL SCORES (%) OF DIFFERENT SCALES OF QUERY OBJECTS BASED ON THE MIT BACKBONE.

Sizes	Methods	COCO-VOC				LVIS			
		O-R@1	O-mAP	I-R@1	I-mAP	O-R@1	O-mAP	I-R@1	I-mAP
[0,20 × 20]	STML [14]	11.85	1.39	18.67	12.75	16.18	2.36	17.49	20.68
	MS-UGCML	15.19	1.71	22.24	16.45	21.67	3.01	22.80	25.78
[20 × 20,30 × 30]	STML [14]	34.82	4.55	43.88	35.67	42.99	5.56	44.59	49.30
	MS-UGCML	46.11	3.72	52.56	47.93	57.16	7.03	58.39	62.55
[30 × 30,60 × 60]	STML [14]	54.33	11.07	63.39	52.57	61.55	7.93	63.27	68.25
	MS-UGCML	68.33	8.78	73.97	67.92	71.35	8.83	72.20	76.56
[60 × 60,100 × 100]	STML [14]	67.86	19.39	77.06	65.58	66.30	10.41	70.39	74.52
	MS-UGCML	80.86	18.25	85.61	79.11	79.04	11.03	80.31	84.15
[100 × 100,~]	STML [14]	78.72	29.15	86.41	80.10	72.51	15.54	77.61	82.67
	MS-UGCML	87.86	31.39	91.02	87.98	83.93	16.65	86.17	90.16

TABLE V
RETRIEVAL SCORES (%) AT BOTH THE OBJECT LEVEL (O-) AND IMAGE LEVEL (I-) ON DIFFERENT DATASETS.

Backbone	Methods	BelgaLogos	Visual Genome				LVIS			
			I-mAP	O-Recall@1	O-mAP	I-Recall@1	I-mAP	O-Recall@1	O-mAP	I-Recall@1
GoogLeNet [50]	STML [14]	63.61	31.82	28.56	31.19	43.54	55.79	6.72	56.57	60.42
	MS-UGCML	65.93	34.01	30.39	34.11	46.93	58.75	7.55	59.75	63.47
MiT-B2 [51]	STML [14]	62.71	26.88	25.26	28.34	43.10	49.31	7.48	51.65	56.14
	MS-UGCML	64.59	33.39	31.95	33.59	46.80	56.83	8.37	58.11	61.96
MoCo-V3 [12]	MoCo-V3 [12]	86.32	43.13	39.47	44.07	67.33	64.95	11.04	67.12	71.51
	MS-UGCML	86.69	42.77	38.95	43.67	66.67	65.14	11.19	67.10	71.59
ViT-B/16 [48]	CLIP [49]	82.01	33.15	30.11	33.62	51.28	55.28	8.51	57.07	61.45
	MS-UGCML	83.73	33.41	30.35	33.75	51.80	55.69	8.70	57.44	61.95

TABLE VI

RETRIEVAL SCORES (%) AT BOTH THE OBJECT LEVEL (O-) AND IMAGE LEVEL (I-) WITH DIFFERENT CLUSTERING NUMBERS ON THE OBJECT RETRIEVAL VALIDATION SET.

Cluster Number	O-Recall@1	O-mAP	I-Recall@1	I-mAP
50	70.43	17.95	74.42	72.47
100	70.60	18.25	74.69	72.47
200	69.98	17.75	74.11	71.99
1000	69.13	17.28	73.07	70.87

that the best performance is achieved when the number of clusters is set to 100.

(2) **Impact of the MS-UGCML group number.** We assessed the effect of the number of groups on the performance of the MS-UGCML method, with the cluster number fixed at 100. The results on the validation set are displayed in Tab. VII, and they indicate that the best performance is attained when the number of groups is set to 4. Thus, in all of our experiments, we set the number of groups as 4.

TABLE VII
RETRIEVAL SCORES (%) AT BOTH THE OBJECT LEVEL (O-) AND IMAGE LEVEL (I-) WITH DIFFERENT GROUP NUMBERS ON THE OBJECT RETRIEVAL VALIDATION SET.

Group Number	O-Recall@1	O-mAP	I-Recall@1	I-mAP
2	70.16	17.74	75.05	72.57
3	70.60	18.25	74.69	72.47
4	70.78	18.25	74.91	72.60
5	69.68	17.75	73.92	71.72

(3) **Impact of the MS-UGCML method.** We assessed the influence of the MS-UGCML method on the object retrieval validation set. Results comparing its use with and without the MS-UGCML method are presented in Tab. VIII, demonstrating an improvement in performance when integrating the MS-UGCML method.

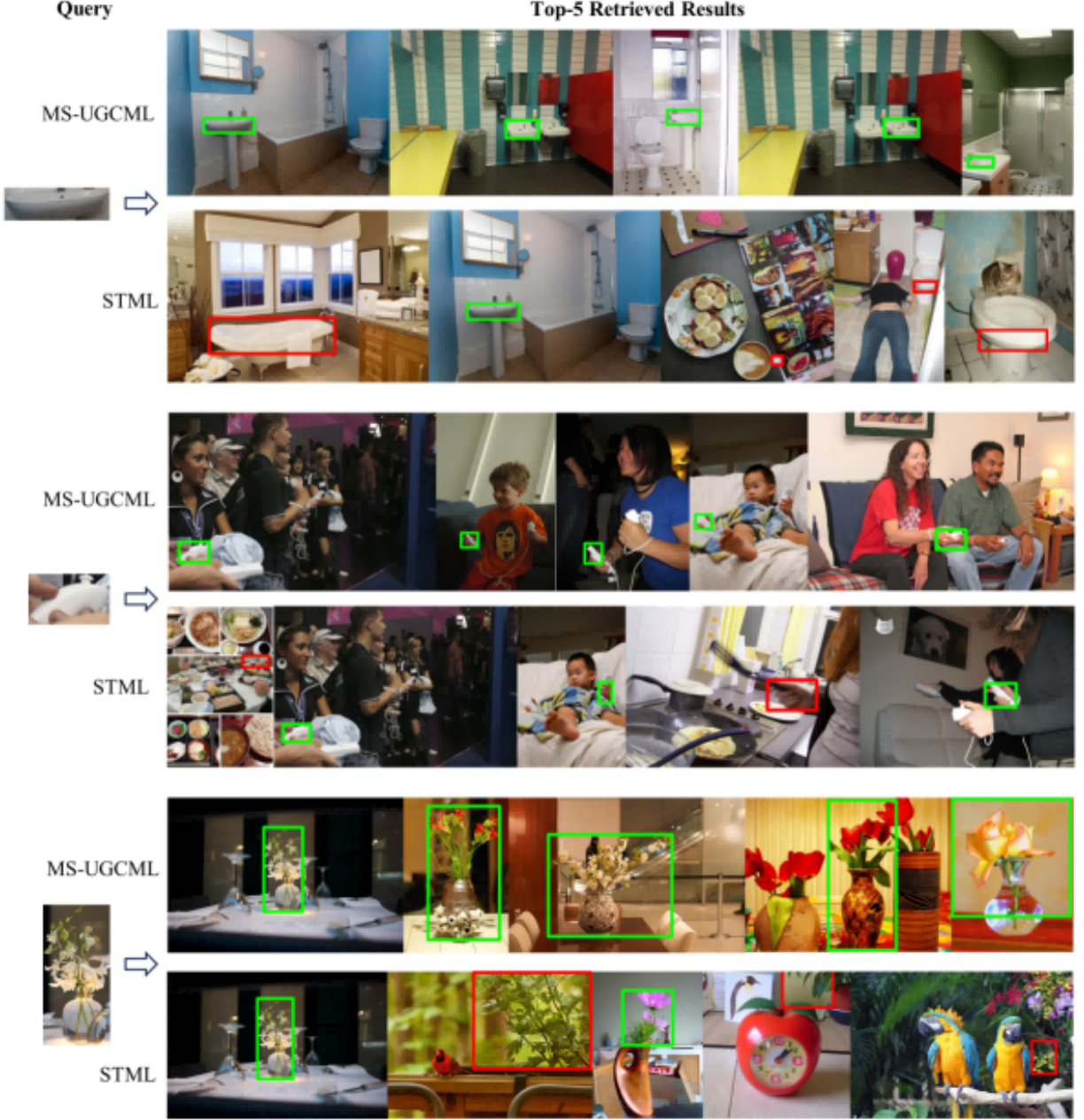


Fig. 7. The comparison of three object retrieval examples between the MS-UGCML and STML [14] methods. Retrieved objects with green boxes are correct ones with the same class label as the query object. Those with red boxes are incorrect results.

TABLE VIII

RETRIEVAL SCORES (%) AT BOTH THE OBJECT LEVEL (O-) AND IMAGE LEVEL (I-) WITH AND WITHOUT USING THE MS-UGCML METHOD ON THE OBJECT RETRIEVAL VALIDATION SET.

Methods	O-Recall@1	O-mAP	I-Recall@1	I-mAP
STML [14]	69.1	16.8	73.1	70.2
+MS-UGCML	70.78	18.25	74.91	72.60

F. More Retrieval Examples

In Fig. 9, we present six retrieval examples. These examples were retrieved using the fine-tuned model based on the MS-UGCML method with parameters initialized using MoCo-V3 [12]. During retrieval, the top five images containing the query object were retrieved. Subsequently, object localization was

conducted in these retrieved images using a similarity score (feature distance).

Fig. 10 shows two failure cases, the first line of the query image in the Fig. 10 is antenna, but the search returns ski-pole and mast. This is because antenna, ski-pole and mast are essentially the same in shape, and distinguishing between them requires more contextual semantic information. The image retrieved in the second row is the BASE logo. However, the fourth image is not the BASE logo, but other text patterns.

VI. CONCLUSION

In this paper, we have addressed the challenges associated with general object retrieval by introducing the mixed-scale group collaborative metric learning (MS-UGCML) method.

TABLE IX

CATEGORY SPLITS FOR THE OPEN-VOCABULARY SCENARIO ARE PROVIDED. KNOWN CLASSES ARE HIGHLIGHTED IN LIGHT YELLOW, WHILE UNKNOWN CLASSES ARE HIGHLIGHTED IN LIGHT BLUE.

Task1											
person	bicycle	car	motorcycle	airplane	bus	train	boat	bird	cat		
dog	horse	sheep	cow	bottle	chair	couch	potted plant	dining table	tv		
truck	traffic light	fire hydrant	stop sign	parking meter	bench	elephant	bear	zebra	giraffe		
backpack	umbrella	handbag	tie	suitcase	microwave	oven	toaster	sink	refrigerator		
frisbee	skis	snowboard	sports ball	kite	baseball bat	baseball glove	skateboard	surfboard	tennis racket		
banana	apple	sandwich	orange	broccoli	carrot	hot dog	pizza	donut	cake		
bed	toilet	laptop	mouse	remote	keyboard	cell phone	book	clock	vase		
scissors	teddy bear	hair drier	toothbrush	wine glass	cup	fork	knife	spoon	bowl		
Task2											
person	bicycle	car	motorcycle	airplane	bus	train	boat	bird	cat		
dog	horse	sheep	cow	bottle	chair	couch	potted plant	dining table	tv		
truck	traffic light	fire hydrant	stop sign	parking meter	bench	elephant	bear	zebra	giraffe		
backpack	umbrella	handbag	tie	suitcase	microwave	oven	toaster	sink	refrigerator		
frisbee	skis	snowboard	sports ball	kite	baseball bat	baseball glove	skateboard	surfboard	tennis racket		
banana	apple	sandwich	orange	broccoli	carrot	hot dog	pizza	donut	cake		
bed	toilet	laptop	mouse	remote	keyboard	cell phone	book	clock	vase		
scissors	teddy bear	hair drier	toothbrush	wine glass	cup	fork	knife	spoon	bowl		
Task3											
person	bicycle	car	motorcycle	airplane	bus	train	boat	bird	cat		
dog	horse	sheep	cow	bottle	chair	couch	potted plant	dining table	tv		
truck	traffic light	fire hydrant	stop sign	parking meter	bench	elephant	bear	zebra	giraffe		
backpack	umbrella	handbag	tie	suitcase	microwave	oven	toaster	sink	refrigerator		
frisbee	skis	snowboard	sports ball	kite	baseball bat	baseball glove	skateboard	surfboard	tennis racket		
banana	apple	sandwich	orange	broccoli	carrot	hot dog	pizza	donut	cake		
bed	toilet	laptop	mouse	remote	keyboard	cell phone	book	clock	vase		
scissors	teddy bear	hair drier	toothbrush	wine glass	cup	fork	knife	spoon	bowl		
Task4											
person	bicycle	car	motorcycle	airplane	bus	train	boat	bird	cat		
dog	horse	sheep	cow	bottle	chair	couch	potted plant	dining table	tv		
truck	traffic light	fire hydrant	stop sign	parking meter	bench	elephant	bear	zebra	giraffe		
backpack	umbrella	handbag	tie	suitcase	microwave	oven	toaster	sink	refrigerator		
frisbee	skis	snowboard	sports ball	kite	baseball bat	baseball glove	skateboard	surfboard	tennis racket		
banana	apple	sandwich	orange	broccoli	carrot	hot dog	pizza	donut	cake		
bed	toilet	laptop	mouse	remote	keyboard	cell phone	book	clock	vase		
scissors	teddy bear	hair drier	toothbrush	wine glass	cup	fork	knife	spoon	bowl		



Fig. 8. Logo retrieval example on the BelgaLogos using the proposed MS-UGCML method.

We have established a comprehensive training and evaluation pipeline using the COCO 2017 and VOC 2007 datasets. Our experiments encompass different backbone networks and initialization methods, with evaluations conducted on BelgaLogos, Visual Genome, and LVIS datasets. The results demonstrate the effectiveness of the proposed MS-UGCML method in enhancing object retrieval performance in open-world scenarios. Nevertheless, there remains substantial room for improvement in general object retrieval, as the target objects typically constitute a relatively small and unpredictable portion of an image, thereby impacting the overall object

retrieval performance.

REFERENCES

- [1] Y. Jiang, J. Meng, J. Yuan, and J. Luo, "Randomized spatial context for object search," *IEEE Transactions on Image Processing*, vol. 24, no. 6, pp. 1748–1762, 2015.
- [2] G. Tolias, R. Sicre, and H. Jégou, "Particular object retrieval with integral max-pooling of cnn activations," in *ICLR 2016-International Conference on Learning Representations*, 2016, pp. 1–12.
- [3] S. Kan, Y. Cen, Z. He, Z. Zhang, L. Zhang, and Y. Wang, "Supervised deep feature embedding with handcrafted feature," *IEEE Transactions on Image Processing*, vol. 28, no. 12, pp. 5809–5823, 2019.
- [4] Y. Zhang, S. Wang, S. Kan, Z. Weng, Y. Cen, and Y.-p. Tan, "Poar: Towards open vocabulary pedestrian attribute recognition," in *ACM MUltimedia 2023*, 2023, pp. 1–10.
- [5] Y. Zhang, F. Zhang, Y. Jin, Y. Cen, V. Voronin, and S. Wan, "Local correlation ensemble with gen based on attention features for cross-domain person re-id," *ACM Transactions on Multimedia Computing, Communications and Applications*, vol. 19, no. 2, pp. 1–22, 2023.
- [6] S. Kan, Z. He, Y. Cen, Y. Li, V. Mladenovic, and Z. He, "Contrastive bayesian analysis for deep metric learning," *IEEE Transactions on Pattern Analysis and Machine Intelligence*, 2022.
- [7] S. Kan, Y. Liang, M. Li, Y. Cen, J. Wang, and Z. He, "Coded residual transform for generalizable deep metric learning," *Advances in Neural Information Processing Systems*, vol. 35, pp. 28 601–28 615, 2022.
- [8] S. Kan, Y. Cen, Y. Li, M. Vladimir, and Z. He, "Local semantic correlation modeling over graph neural networks for deep feature embedding and image retrieval," *IEEE Transactions on Image Processing*, vol. 31, pp. 2988–3003, 2022.
- [9] Z. Liu, Z. Miao, X. Zhan, J. Wang, B. Gong, and X. Y. Stella, "Open long-tailed recognition in a dynamic world," *IEEE Transactions on Pattern Analysis and Machine Intelligence*, 2022.

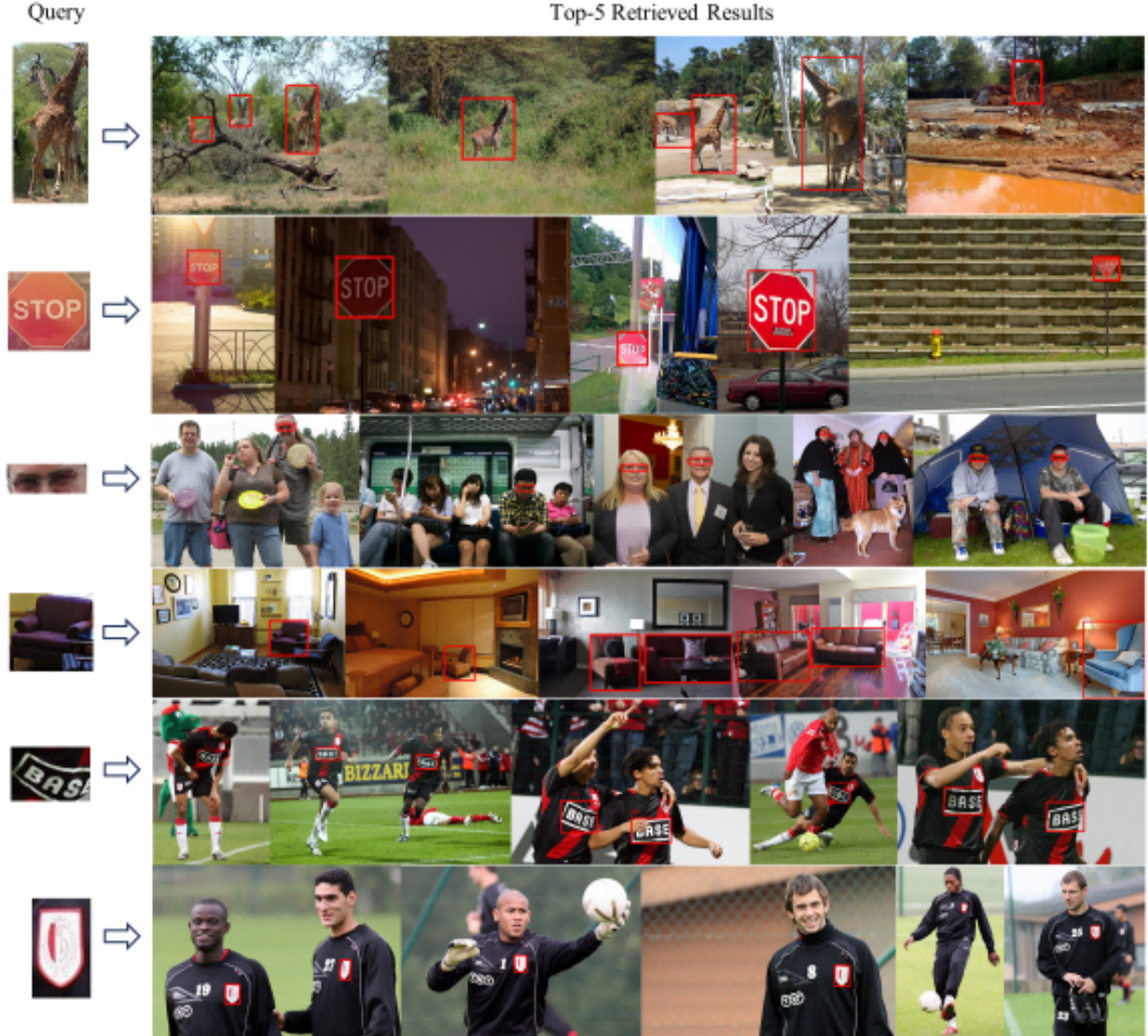


Fig. 9. Six object retrieval examples using the fine-tuned model based on the MS-UGCML method with parameters initialized using MoCo-V3.

- [10] A. Kirillov, E. Mintun, N. Ravi, H. Mao, C. Rolland, L. Gustafson, T. Xiao, S. Whitehead, A. C. Berg, W.-Y. Lo *et al.*, “Segment anything,” *arXiv preprint arXiv:2304.02643*, 2023.
- [11] M. Caron, H. Touvron, I. Misra, H. Jégou, J. Mairal, P. Bojanowski, and A. Joulin, “Emerging properties in self-supervised vision transformers,” in *Proceedings of the IEEE/CVF international conference on computer vision*, 2021, pp. 9650–9660.
- [12] X. Chen, S. Xie, and K. He, “An empirical study of training self-supervised vision transformers,” in *2021 IEEE/CVF International Conference on Computer Vision (ICCV)*, 2021, pp. 9620–9629.
- [13] J. Zhou, C. Wei, H. Wang, W. Shen, C. Xie, A. Yuille, and T. Kong, “ibot: Image bert pre-training with online tokenizer,” *arXiv preprint arXiv:2111.07832*, 2021.
- [14] S. Kim, D. Kim, M. Cho, and S. Kwak, “Self-taught metric learning without labels,” in *Proceedings of the IEEE/CVF Conference on Computer Vision and Pattern Recognition*, 2022, pp. 7431–7441.
- [15] M. Maaz, H. Rasheed, S. Khan, F. S. Khan, R. M. Anwer, and M.-H. Yang, “Class-agnostic object detection with multi-modal transformer,” in *European Conference on Computer Vision*. Springer, 2022, pp. 512–531.
- [16] O. Russakovsky, J. Deng, H. Su, J. Krause, S. Satheesh, S. Ma, Z. Huang, A. Karpathy, A. Khosla, M. Bernstein *et al.*, “Imagenet large scale visual recognition challenge,” *International journal of computer vision*, vol. 115, pp. 211–252, 2015.
- [17] H. Oh Song, Y. Xiang, S. Jegelka, and S. Savarese, “Deep metric learning via lifted structured feature embedding,” in *Proceedings of the IEEE conference on computer vision and pattern recognition*, 2016, pp. 4004–4012.
- [18] C. Wah, S. Branson, P. Welinder, P. Perona, and S. Belongie, “The caltech-ucsd birds-200-2011 dataset,” 2011.
- [19] J. Krause, M. Stark, J. Deng, and L. Fei-Fei, “3d object representations for fine-grained categorization,” in *Proceedings of the IEEE international conference on computer vision workshops*, 2013, pp. 554–561.
- [20] J. Philbin, O. Chum, M. Isard, J. Sivic, and A. Zisserman, “Object retrieval with large vocabularies and fast spatial matching,” in *2007 IEEE conference on computer vision and pattern recognition*. IEEE, 2007, pp. 1–8.
- [21] ———, “Lost in quantization: Improving particular object retrieval in large scale image databases,” in *2008 IEEE conference on computer vision and pattern recognition*, 2008, pp. 1–8.
- [22] T.-Y. Lin, M. Maire, S. Belongie, J. Hays, P. Perona, D. Ramanan, P. Dollár, and C. L. Zitnick, “Microsoft coco: Common objects in context,” in *Computer Vision-ECCV 2014: 13th European Conference, Zurich, Switzerland, September 6–12, 2014, Proceedings, Part V 13*. Springer, 2014, pp. 740–755.
- [23] M. Everingham, “The pascal visual object classes challenge 2007 (voc2007) results,” in <http://host.robots.ox.ac.uk/pascal/VOC/voc2007/>, 2007.
- [24] A. Joly and O. Buisson, “Logo retrieval with a contrario visual query expansion,” in *Proceedings of the 17th ACM international conference on Multimedia*, 2009, pp. 581–584.
- [25] R. Krishna, Y. Zhu, O. Groth, J. Johnson, K. Hata, J. Kravitz, S. Chen,



Fig. 10. Two failure cases. The first line of the query image is antenna, but the search returns ski-pole and mast. The image retrieved in the second row is the BASE logo. However, the fourth image is not the BASE logo, but other text patterns.

Y. Kalantidis, L.-J. Li, D. A. Shamma *et al.*, “Visual genome: Connecting language and vision using crowdsourced dense image annotations,” *International journal of computer vision*, vol. 123, pp. 32–73, 2017.

[26] A. Gupta, P. Dollar, and R. Girshick, “Lvis: A dataset for large vocabulary instance segmentation,” in *Proceedings of the IEEE/CVF conference on computer vision and pattern recognition*, 2019, pp. 5356–5364.

[27] Sivic and Zisserman, “Video google: A text retrieval approach to object matching in videos,” in *Proceedings ninth IEEE international conference on computer vision*. IEEE, 2003, pp. 1470–1477.

[28] H. Jégou, F. Perronnin, M. Douze, J. Sánchez, P. Pérez, and C. Schmid, “Aggregating local image descriptors into compact codes,” *IEEE transactions on pattern analysis and machine intelligence*, vol. 34, no. 9, pp. 1704–1716, 2011.

[29] Y. Zhang, Z. Jia, and T. Chen, “Image retrieval with geometry-preserving visual phrases,” in *CVPR 2011*. IEEE, 2011, pp. 809–816.

[30] S. Zhang, Q. Huang, G. Hua, S. Jiang, W. Gao, and Q. Tian, “Building contextual visual vocabulary for large-scale image applications,” in *Proceedings of the 18th ACM international conference on Multimedia*, 2010, pp. 501–510.

[31] G. Tolias, R. Sicre, and H. Jégou, “Particular object retrieval with integral max-pooling of cnn activations,” in *ICLR 2016-International Conference on Learning Representations*, 2016, pp. 1–12.

[32] R. Hadsell, S. Chopra, and Y. LeCun, “Dimensionality reduction by learning an invariant mapping,” in *2006 IEEE computer society conference on computer vision and pattern recognition (CVPR’06)*, vol. 2. IEEE, 2006, pp. 1735–1742.

[33] F. Schroff, D. Kalenichenko, and J. Philbin, “Facenet: A unified embedding for face recognition and clustering,” in *Proceedings of the IEEE conference on computer vision and pattern recognition*, 2015, pp. 815–823.

[34] X. Wang, X. Han, W. Huang, D. Dong, and M. R. Scott, “Multi-similarity loss with general pair weighting for deep metric learning,” in *Proceedings of the IEEE/CVF conference on computer vision and pattern recognition*, 2019, pp. 5022–5030.

[35] K. He, H. Fan, Y. Wu, S. Xie, and R. Girshick, “Momentum contrast for unsupervised visual representation learning,” in *Proceedings of the IEEE/CVF conference on computer vision and pattern recognition*, 2020, pp. 9729–9738.

[36] T. Chen, S. Kornblith, M. Norouzi, and G. Hinton, “A simple framework for contrastive learning of visual representations,” in *International conference on machine learning*. PMLR, 2020, pp. 1597–1607.

[37] B. X. Nguyen, B. D. Nguyen, G. Carneiro, E. Tjiputra, Q. D. Tran, and T.-T. Do, “Deep metric learning meets deep clustering: An novel unsupervised approach for feature embedding,” *arXiv preprint arXiv:2009.04091*, 2020.

[38] S. Kan, Y. Cen, Y. Li, V. Mladenovic, and Z. He, “Relative order analysis and optimization for unsupervised deep metric learning,” in *Proceedings of the IEEE/CVF conference on computer vision and pattern recognition*, 2021, pp. 13 999–14 008.

[39] Y. Li, S. Kan, J. Yuan, W. Cao, and Z. He, “Spatial assembly networks for image representation learning,” in *Proceedings of the IEEE/CVF Conference on Computer Vision and Pattern Recognition*, 2021, pp. 13 876–13 885.

[40] J. Sivic and A. Zisserman, “Efficient visual search of videos cast as text retrieval,” *IEEE transactions on pattern analysis and machine intelligence*, vol. 31, no. 4, pp. 591–606, 2008.

[41] C. H. Lampert, “Detecting objects in large image collections and videos by efficient subimage retrieval,” in *2009 IEEE 12th International Conference on Computer Vision*. IEEE, 2009, pp. 987–994.

[42] C. H. Lampert, M. B. Blaschko, and T. Hofmann, “Beyond sliding windows: Object localization by efficient subwindow search,” in *2008 IEEE conference on computer vision and pattern recognition*. IEEE, 2008, pp. 1–8.

[43] C.-Y. Wang, A. Bochkovskiy, and H.-Y. M. Liao, “Yolov7: Trainable bag-of-freebies sets new state-of-the-art for real-time object detectors,” in *Proceedings of the IEEE/CVF Conference on Computer Vision and Pattern Recognition*, 2023, pp. 7464–7475.

[44] R. Girshick, “Fast r-cnn,” in *Proceedings of the IEEE international conference on computer vision*, 2015, pp. 1440–1448.

[45] K. Joseph, S. Khan, F. S. Khan, and V. N. Balasubramanian, “Towards open world object detection,” in *Proceedings of the IEEE/CVF conference on computer vision and pattern recognition*, 2021, pp. 5830–5840.

[46] I. Loshchilov and F. Hutter, “Sgdr: Stochastic gradient descent with warm restarts,” *arXiv preprint arXiv:1608.03983*, 2016.

[47] B. Heo, S. Chun, S. J. Oh, D. Han, S. Yun, G. Kim, Y. Uh, and J.-W. Ha, “Adamp: Slowing down the slowdown for momentum optimizers on scale-invariant weights,” in *International Conference on Learning Representations*, 2021.

[48] A. Dosovitskiy, L. Beyer, A. Kolesnikov, D. Weissenborn, X. Zhai, T. Unterthiner, M. Dehghani, M. Minderer, G. Heigold, S. Gelly *et al.*, “An image is worth 16x16 words: Transformers for image recognition at scale,” *arXiv preprint arXiv:2010.11929*, 2020.

[49] A. Radford, J. W. Kim, C. Hallacy, A. Ramesh, G. Goh, S. Agarwal, G. Sastry, A. Askell, P. Mishkin, J. Clark *et al.*, “Learning transferable visual models from natural language supervision,” in *International conference on machine learning*. PMLR, 2021, pp. 8748–8763.

[50] C. Szegedy, W. Liu, Y. Jia, P. Sermanet, S. Reed, D. Anguelov, D. Erhan, V. Vanhoucke, and A. Rabinovich, “Going deeper with convolutions,” in *Proceedings of the IEEE conference on computer vision and pattern recognition*, 2015, pp. 1–9.

[51] E. Xie, W. Wang, Z. Yu, A. Anandkumar, J. M. Alvarez, and P. Luo, “Segformer: Simple and efficient design for semantic segmentation with transformers,” *Advances in Neural Information Processing Systems*, vol. 34, pp. 12 077–12 090, 2021.



Shichao Kan received the B.E., M.S. and Ph.D. degrees from the School of Computer and Information Science, Beijing Jiaotong University, Beijing, China, in 2014, 2016 and 2021, respectively. From 2019 to 2020, he was a visiting student researcher with the Department of Computer Science, University of Missouri, Columbia, MO, USA. He is currently a lecturer with the School of Computer Science and Engineering, Central South University, Hunan, China. His research interests include metric learning, object retrieval, large-scale image retrieval, and large vision-language model.



Yuhai Deng is a fourth-year student majoring in Intelligence Science and Technology at Central South University, Hunan, China. His research interests lie primarily in computer vision and machine learning, with a particular focus on image retrieval.



Xiong Liang currently holds the position of Professor of Computer Science at Central South University. He served as a visitor at the Robotics Institute, Carnegie Mellon University, from 2011 to 2012, and worked as a Postdoctoral Fellow at the Institute of Automation, Chinese Academy of Sciences, from 2005 to 2007. He obtained his Ph.D., M.S., and B.S. degrees from Chongqing University, China, in 2005, 2002, and 1999, respectively. His research interests include computer vision and machine learning.



Lihui Cen received her B.S. and M.S. degrees from Central South University in 2000 and 2003, respectively. She received her Ph. D. degree from Shanghai Jiaotong University in 2010. Since 2013, she has been an associate professor with School of Information Science and Engineering, Central South University. She is presently a professor of Control Theory and Control Engineering with School of Automation, Central South University. Her research interests cover data-driven modeling, deep learning and their applications.



Zhe Qu received the BS degree from Xiamen University in 2015, the MS degree from the University of Delaware in 2017 and the Ph.D. degree from University of South Florida in 2022. He is currently a tenure-track Associate Professor with the School of Computer Science and Engineering, Central South University, China. His primary research interests include network and mobile system security, and machine learning for networks.



Yigang Cen received the Ph.D. degree in control science engineering from the Huazhong University of Science Technology, Wuhan, China, in 2006. In 2006, he joined the Signal Processing Centre, School of Electrical and Electronic Engineering, Nanyang Technological University, Singapore, as a Research Fellow. From 2014 to 2015, he was a Visiting Scholar with the Department of Computer Science, University of Missouri, Columbia, MO, USA. He is currently a Professor and a Supervisor of doctoral students with the School of Computer and Information Technology, Beijing Jiaotong University, Beijing, China. His research interests include computer vision, intelligent transportation and intelligent security, etc.



Zhihai He (IEEE Fellow 2015) received the B.S. degree in mathematics from Beijing Normal University, Beijing, China, in 1994, the M.S. degree in mathematics from the Institute of Computational Mathematics, Chinese Academy of Sciences, Beijing, China, in 1997, and the Ph.D. degree in electrical engineering from the University of California, at Santa Barbara, Santa Barbara, CA, USA, in 2001. In 2001, he joined Sarnoff Corporation, Princeton, NJ, USA, as a member of technical staff. In 2003, he joined the Department of Electrical and Computer Engineering, University of Missouri, Columbia MO, USA, where he was a Tenured Full Professor. He is currently a chair professor with the Department of Electrical and Electronic Engineering, Southern University of Science and Technology, Shenzhen, P. R. China. His current research interests include image/video processing and compression, wireless sensor network, computer vision, and cyber-physical systems.

He is a member of the Visual Signal Processing and Communication Technical Committee of the IEEE Circuits and Systems Society. He serves as a technical program committee member or a session chair of a number of international conferences. He was a recipient of the 2002 IEEE TRANSACTIONS ON CIRCUITS AND SYSTEMS FOR VIDEO TECHNOLOGY Best Paper Award and the SPIE VCIP Young Investigator Award in 2004. He was the Co-Chair of the 2007 International Symposium on Multimedia Over Wireless in Hawaii. He has served as an Associate Editor for the IEEE TRANSACTIONS ON CIRCUITS AND SYSTEMS FOR VIDEO TECHNOLOGY (TCSVT), the IEEE TRANSACTIONS ON MULTIMEDIA (TMM), and the Journal of Visual Communication and Image Representation. He was also the Guest Editor for the IEEE TCSVT Special Issue on Video Surveillance.